Applied Catalysis B: Environmental 326 (2023) 122338

Contents lists available at ScienceDirect

Applied Catalysis B: Environmental

journal homepage: www.elsevier.com/locate/apcatb

Photocatalytic conversion of carbon dioxide on triethanolamine: Unheeded catalytic performance of sacrificial agent

Zhiguo Liu [a], Jiaying Li [a], Ziyu Chen [a], Mingyang Li [a], Lingzhi Wang [a,b], Shiqun Wu [a,*], Jinlong Zhang [a,b,**]

[a] Shanghai Engineering Research Center for Multi-media Environmental Catalysis and Resource Utilization, Key Laboratory for Advanced Materials and Joint International Research Laboratory of Precision Chemistry and Molecular Engineering, Feringa Nobel Prize Scientist Joint Research Center, Frontiers Science Center for Materiobiology and Dynamic Chemistry, School of Chemistry and Molecular Engineering, East China University of Science and Technology, 130 Meilong Road, Shanghai 200237, PR China

[b] School of Chemistry & Chemical Engineering, Yancheng Institute of Technology, Yancheng 224051, PR China

ARTICLE INFO

Keywords:
Sacrificial agent
CO_2 reduction
Triethanolamine
Photocatalysis

ABSTRACT

Potential catalytic performance of sacrificial agents triethanolamine (TEOA) has not been explored yet, seriously affecting the evaluation of catalyst performance and reaction mechanism. Herein, we report direct evidence of TEOA, a popular sacrificial agent in CO_2 photoreduction, photocatalytic conversion of CO_2 into CO and CH_4 for the first time. Combining experimental and theoretical studies, it is corroborated that TEOA with terminal hydroxyl group as active site serves as a photocatalyst possessing appropriate energy level for the ultraviolet light response. Comprehensive investigations endorsed that the two products of CH_4 and CO are derived from conventional photocatalytic CO_2 hydrogenation and photoinduced homocleavage of RO-COOH followed by a hydrogen atom transfer process, respectively. The current work demonstrates the nonnegligible catalytic influence of TEOA and provides guidance in choosing suitable sacrificial agents during solid–liquid photocatalytic redox reactions.

1. Introduction

Excessive emissions of CO_2-induced global warming have provoked the wide attention of the whole world in recent years.[1–5] Converting solar energy and CO_2 into high-value-added fuels and chemicals through photocatalytic technology is a promising and fast developing route toward a sustainable and carbon-neutral economy. [6–9] In solid-liquid photocatalytic CO_2 reduction reaction (CO_2 RR) systems, two main factors of catalysts and sacrificial agents are known to bolster the catalytic performance of the reaction system. [10–12] Much research so far has focused on constructing and modifying catalysts to enhance CO_2 photoreduction activity and regulate product selectivity. [13–19] Nevertheless, sacrificial agents have received insufficient attention in photocatalysis [20–23].

Triethanolamine (TEOA) is widely used for the economic and efficient enrichment of CO_2 from flue gas (pH > 11, Scheme S1. a) [24, 25] and as an effective sacrificial agent in photocatalytic CO_2 reduction reaction (Scheme S1. b) to improve the efficiency. [26–30] Wang et al. elucidated that TEOA as a sacrificial agent would enable the catalytic system to exhibit the highest photocatalytic CO_2 reduction activity. [31] Ye et al. validated that there are no C-C or C-N bonds broken in TEOA during photocatalytic CO_2 reduction through ^1H nuclear magnetic resonance (NMR) and high-resolution electrospray ionization mass spectrometry (ESI-MS) analysis. [10] In contrast, Sebastian C. Peter et al. recently revealed that TEOA decomposes to produce CO, CH_4, and C_2H_4 when the experimental parameters were 450 W Xenon arc lamp (200–2400 nm). [12] In addition, previous studies on photocatalysis have found that many substances have different effects than expected, and studies have also been conducted on these substances with multiple effects.[32–35] However, no systematic study concerning the TEOA

* Corresponding author.
** Corresponding author at: Shanghai Engineering Research Center for Multi-media Environmental Catalysis and Resource Utilization, Key Laboratory for Advanced Materials and Joint International Research Laboratory of Precision Chemistry and Molecular Engineering, Feringa Nobel Prize Scientist Joint Research Center, Frontiers Science Center for Materiobiology and Dynamic Chemistry, School of Chemistry and Molecular Engineering, East China University of Science and Technology, 130 Meilong Road, Shanghai 200237, PR China.
E-mail addresses: wushiqun@ecust.edu.cn (S. Wu), jlzhang@ecust.edu.cn (J. Zhang).

https://doi.org/10.1016/j.apcatb.2022.122338
Received 15 December 2022; Received in revised form 24 December 2022; Accepted 27 December 2022
Available online 11 January 2023

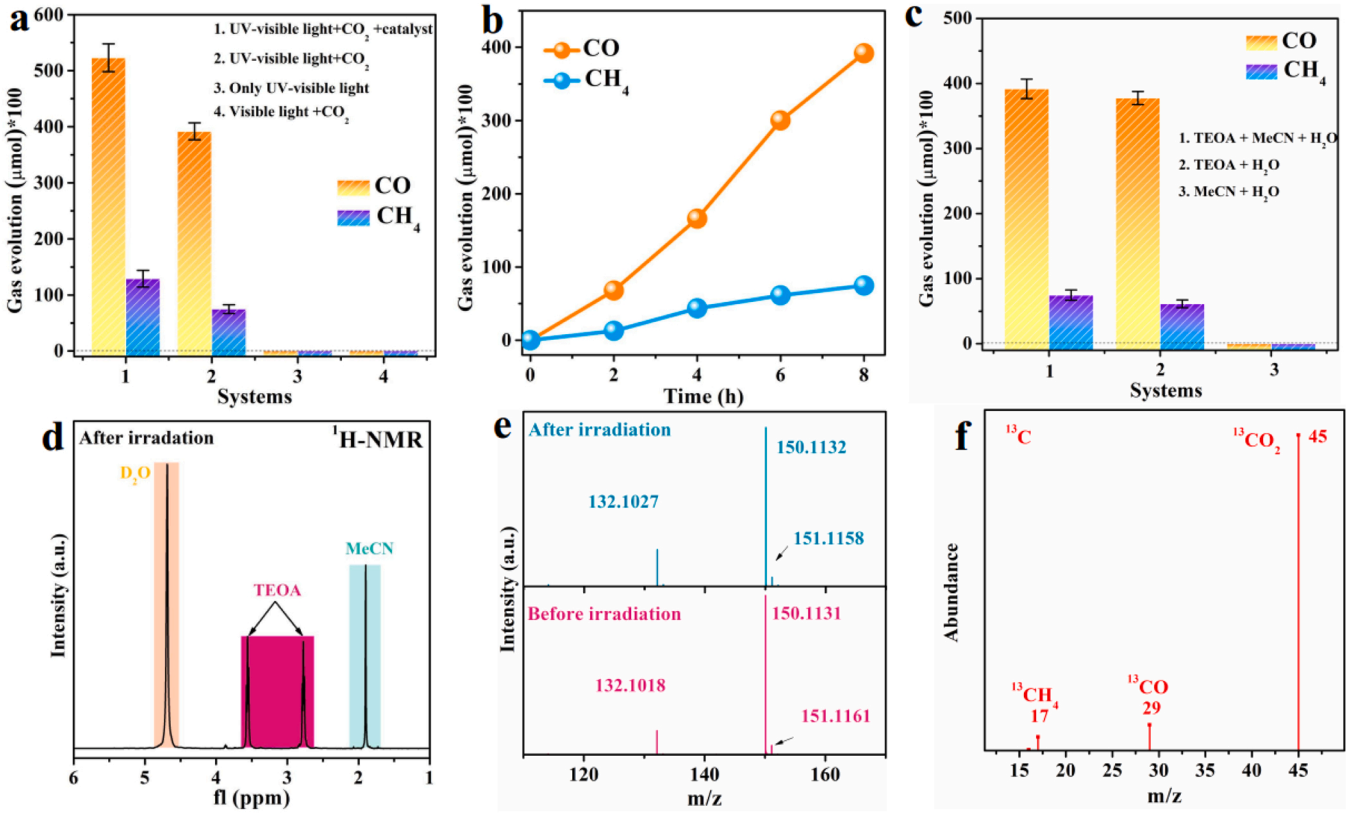

Fig. 1. (a) The generation rate of the CO_2 reduction reaction product under different conditions (1: under UV–visible light irradiation with catalyst, TEOA, MeCN, H_2O, and CO_2; 2: under UV–visible light irradiation with TEOA, MeCN, H_2O, and CO_2; 3: under UV–visible light irradiation with TEOA, MeCN, and H_2O; 4: under visible light irradiation with catalyst, TEOA, MeCN, H_2O, and CO_2). (b) Photocatalytic CO_2 reduction reaction point plots for producing CH_4 and CO (System 2 in Fig. 1a). (c) Photocatalytic CO_2 reduction reaction performance with or without MeCN/TEOA. (d) ^{1}H NMR spectra after light irradiation. (e) ESI-MS spectra before and after light irradiation. (f) Gas Chromatography-Mass Spectrometer (GC-MS) spectra of ^{13}CO, and $^{13}CH_4$ from the photocatalytic reduction of $^{13}CO_2$ on TEOA.

decomposition path and mechanism at the molecular level was provided. Consequently, exploring the role of TEOA in photocatalytic CO_2 reduction under different reaction conditions can provide deep insight into the catalytic mechanism of CO_2 conversion. Furthermore, in addition to the sacrificial agent effect and self-decomposition effect of TEOA, the potential catalytic influence of TEOA has not been explored before, which cannot be ignored due to the complex reaction system and low overall yield of photocatalytic CO_2 reduction.

Herein, we report for the first time that TEOA not only acts as a hole trapping agent but also exhibits photocatalytic activity in the process of photocatalytic CO_2 reduction reaction. ^{1}H NMR and ESI-MS validated the structural stability of TEOA during the process of CO_2 photoreduction. The electronic structure of TEOA satisfies CO_2 photoreduction with the terminal hydroxyl group as the active site was corroborated by DFT calculations. Crucially, combining the reaction path calculation of Gibbs free energy and the control experiments, the main reaction paths of CH_4 and CO production are investigated.

2. Experimental section

2.1. Chemicals

The chemicals we used in this work included triethanolamine ($C_6H_{15}NO_3$, TEOA, AR), methyl cyanide (C_2H_3N, MeCN, HPLC), $NaHCO_3$ (AR), formic acid (HCOOH, AR), isopropanol (C_3H_8O, AR), oxalic acid ($H_2C_2O_4$, AR), ascorbic acid ($C_6H_8O_6$, AR), melamine ($C_3H_6N_6$, AR), methanol (CH_3OH, HPLC), ethanol (C_2H_5OH, HPLC), ultrahigh purity CO_2 (99.99%), ultrahigh purity $^{13}CO_2$ (99.52 atom% ^{13}C), triethylamine ($C_6H_{15}N$, TEA, AR), and deuterium water (D_2O, 99.9%). Ultrapure water was purchased without any further purification.

2.2. Photocatalytic CO_2 reduction

The photocatalytic CO_2 reaction was analyses with an all-glass automatic online trace gas analysis system (Labsolar-6A, Beijing Perfectlight). First, 4 mL of deionized water, 4 mL of triethanolamine (TEOA), and 12 mL of acetonitrile (MeCN) solution were added to the reactor (250 mL volume with a quartz cover). After mixing with stirring and ultrasound, the reaction system was vacuumed, and CO_2 (99.99%) at approximately 1 atm (315 mL) was introduced through a flow meter. The above cleaning process was repeated three times to remove as much air from the reaction system as possible. Water was poured into the outer wall of the reactor, and the temperature of the entire reaction system was kept stable at 10 or 25 °C. Under light irradiation (a 300 W Xeon lamp coupled with a 280–780 nm filter was used as the light source), the gas products were passed into a gas chromatograph (GC, Fuli Instruments, China, GC-9790 Plus) for detection. Carbon-containing products such as methane, carbon monoxide, methanol, and multicarbon products were analyses by flame ionization detector (FID), and other hydrogen, oxygen, and nitrogen were detected by thermal conductivity detector (TCD). Error bars represent the standard deviation of three independent measurements using fresh samples for each measurement. In the test of adding PCN as a catalyst, PCN was added when TEOA, MeCN, and H_2O were uniformly mixed by ultrasonication, and there was no difference in other test steps. $^{13}CO_2$ isotope labeling experiments were conducted under the same conditions, and the gas products were quantified by GC-MS (gas chromatography-mass spectrometry, Japan, QP2010 plus) with a triple-axis detector. The calibration of gas chromatography and the original spectrum of gas

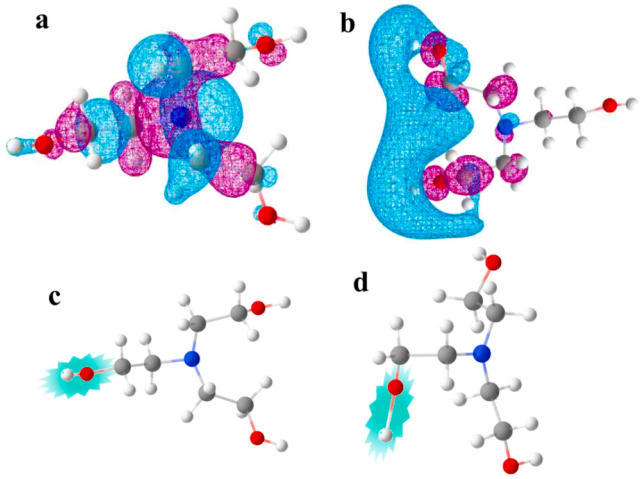

Fig. 2. Frontier orbitals of TEOA in the S_0 geometry. (a) HOMO and (b) LUMO. (c) Ground state and (d) excited the state of TEOA.

chromatography are shown in Fig. S1-S3.

3. Results and discussion

3.1. CO_2 reduction reaction performance evaluation

Polymeric carbon nitride (PCN) is employed as the photocatalyst, which is successfully prepared by gradient heating melamine at 550 °C. The photocatalytic performance for solid–liquid CO_2 reduction reaction is evaluated under different conditions. As shown in Fig. 1a, the photocatalytic performance of system 1 is detected under UV–visible (280–780 nm) irradiation with catalyst (PCN) and CO_2. The products are mainly composed of CO (523 μmol·g^{-1}) and CH_4 (129 μmol·g^{-1}). Interestingly, the photocatalytic activity of the system can still be maintained at 75% when the catalyst is removed (Fig. 1a, system 2). In this scenario, two possibilities are speculated: (1) the organic solvent (TEOA and MeCN) decomposes to produce CO and CH_4; (2) CO_2 is reduced by the solvent (TEOA and MeCN) in the absence of a conventional catalyst. To corroborate the reaction path, comparative experiments were carried out. System 3 without CO_2 confirmed that the organic solvents cannot be decomposed into gaseous products, excluding possibility 1. As shown in Fig. 1c, the yields of CO and CH_4 hardly changed between systems 1 and 2, verifying a negligible contribution of MeCN. In contrast, both CO and CH_4 were no longer produced without TEOA, confirming its ability to photoreduce CO_2. Thereby, it is proved that the effective "catalyst" in the organic solvent is TEOA. Moreover, other commonly used sacrificial agents (triethylamine, methanol, ethanol, isopropanol, ascorbic acid, oxalic acid, formic acid, and $NaHCO_3$) show no activity toward CO_2 photoreduction (Fig. S4). Meanwhile, no product was produced (system 4) when using a visible light source (400–780 nm), demonstrating the necessity of UV light for CO_2 conversion by TEOA. Fig. 1b shows the photocatalytic CO_2 reduction reaction point plots of products CO and CH_4 (system 2), exhibiting a quasi-linear plot of CO and CH_4 generation with reaction time, further proving the product comes from catalytic reduction. The influences of temperature and light intensity on photocatalytic performance are investigated, as shown in Fig. S5. The production rate is significantly affected by light intensity and temperature, exhibiting similar characteristics to the catalytic reduction process by the catalyst [25].

To further exclude the possibility of TEOA self-decomposition under light illumination, a comparative experiment was carried out. [12] The ^{1}H NMR spectra of MeCN and TEOA are shown in Fig. S6, in which the peak attributed to MeCN is located at 1.98 ppm, while the peaks of TEOA are located at 2.57, 3.42, and 4.16 ppm. The possibility of a C-C bond and C-N cleavage (Fig. S6c and S6d) with peaks of 2.18 and 5.9 ppm were not found in the ^{1}H NMR spectrum after light irradiation (Fig. 1d), indicating the outstanding stability of TEOA. Moreover, no changes were detectable after light irradiation of TEOA confirmed by EIS-MS, further validating the stability of TEOA under light illumination (Fig. 1e). The isotope-labeled $^{13}CO_2$ experiment was also conducted under the same experimental conditions to directly confirm the source of products. The Gas Chromatography-Mass Spectrometer (GC−MS) peak sequenced of CO, CH_4, and MeCN are shown in Fig. S7. The ion fragment analysis results of each peak are displayed in Fig. 1f. The relatively abundance of $m/z = 17$ ($^{13}CH_4$) and $m/z = 29$ (^{13}CO) can be clearly seen

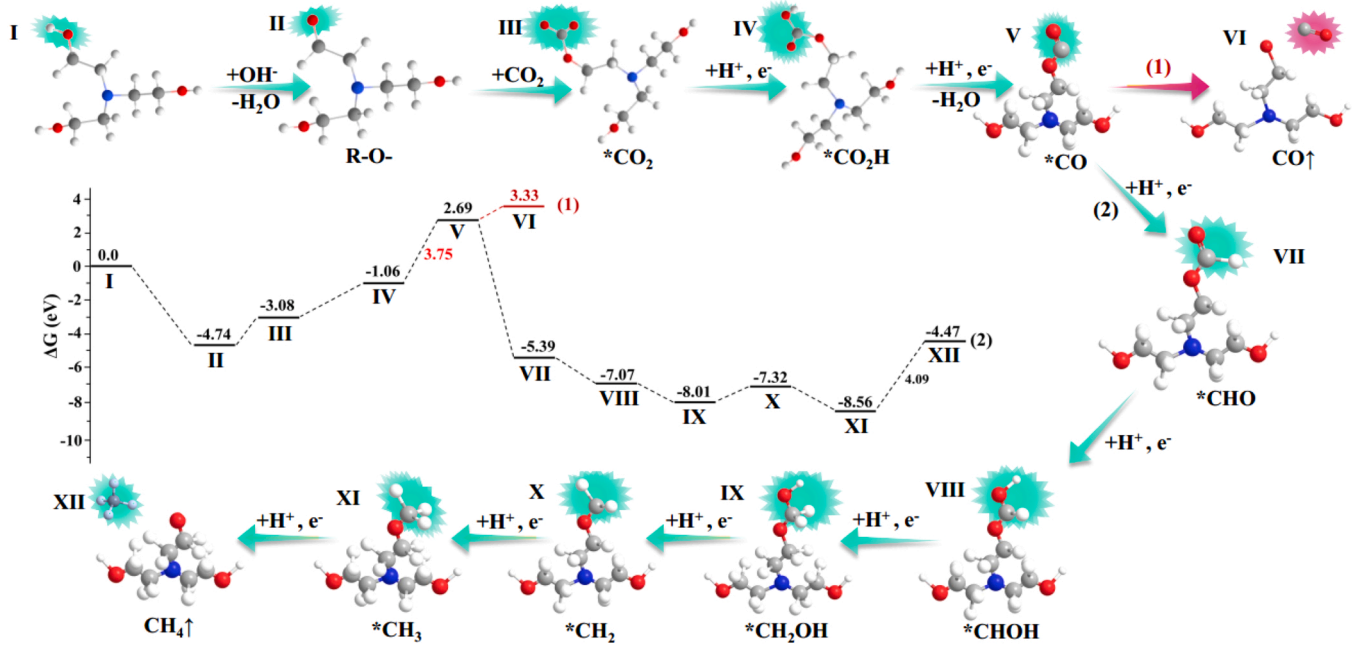

Fig. 3. One RO^- group as an active site. Calculated Gibbs free energy diagram for CO_2 reduction towards CO and CH_4 over TEOA and the corresponding optimized structure of each step in the whole reaction. The blue, red, gray, and white balls represent N, O, C, and H atoms, respectively.

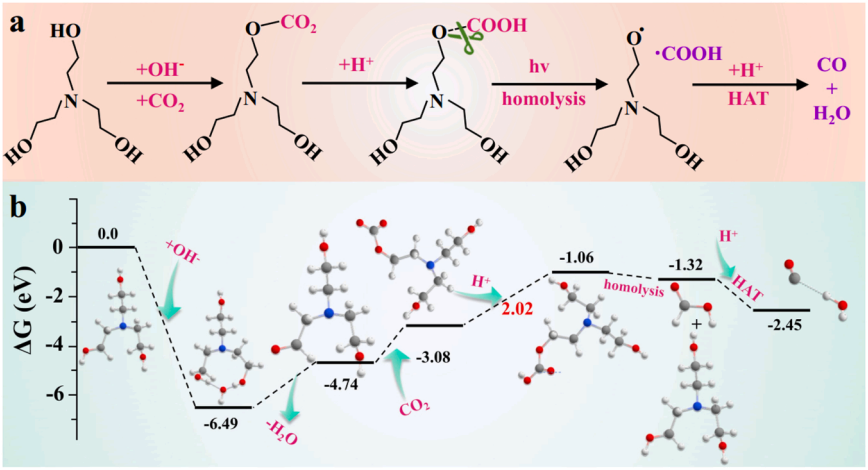

Fig. 4. (a) Schematic diagram of the mechanism of TEOA catalyzing CO_2 to CO via the HAT process; (b) calculated Gibbs free energy diagram for HAT and the corresponding optimized structure of each step in the whole reaction. The blue, red, gray, and white balls represent N, O, C, and H atoms, respectively.

without the signal appearances of ^{12}CO and $^{12}CH_4$. Therefore, it can be concluded that the products of CO and CH_4 are derived from the photocatalytic CO_2 conversion process by TEOA.

3.2. OH acts as the active site of CO_2 reduction reaction

The electronic structure and active site of TEOA is a vital prerequisite to CO_2 photoreduction. [11,36] In the ground (S_0) states, the HOMO orbitals are mainly contributed by the atomic orbitals near the N atom (Fig. 2a), while the LUMO orbitals (Fig. 2b) are composed of the hydroxyl groups at the endpoints. The molecular orbitals near the HOMO frontier are mainly contributed by the p orbitals, and the s orbitals are mainly involved in the formation of the LUMO orbitals according to the density of states (DOS, Fig. S8b). It can be obtained that orbits No. 41 and No. 42 are the highest occupied orbital (HOMO) and lowest unoccupied orbital (LUMO), respectively, according to the specific orbital distribution energy map (Fig. S8c). The HOMO and LUMO obtained by the conversion are 2.87 and −0.64 eV, indicating a 3.51 eV bandgap of TEOA. Furthermore, the absorption band edge of TEOA is detected as 350 nm, corresponding to a bandgap of 3.54 eV (Fig. S8a), coinciding with the theoretical calculation. Combining theoretical calculations and experimental verification, the electronic energy level distribution of TEOA is obtained (Fig. S8d). The LUMO energy level can satisfy the requirement of CO_2 reduction, [37] providing theoretical feasibility of TEOA to catalyze CO_2 reduction under UV light irradiation.

To gain insight into the active sites of TEOA for CO_2 photoreduction, the structural changes of TEOA in the ground and excited states are investigated through simulation calculations (Fig. 2c and 2d). In the excited state, the terminal O-H bond of the C-O-H group is elongated, which is conducive to the reaction of hydrogen and hydroxyl to form a C-O^- active site. Moreover, CO_2 reduction by triethylamine (TEA) was almost inactive (Fig. S4), suggesting that the terminal hydroxyl group is the active site since TEA possesses a structure similar to that of TEOA except lacking a terminal hydroxyl group. Therefore, the terminal hydroxyl group is determined to be the active site of TEOA for CO_2 photoreduction.

3.3. Conventional photocatalytic CO_2 hydrogenation

In situ Fourier transform infrared spectroscopy (FTIR) measurements and DFT calculations were carried out to explore the CO_2 reduction route and mechanism of TEOA. Several complex bands are observed in the regions 1100–3100 cm^{-1} as shown in Fig. S9 and S10. The Gibbs energy diagrams of the CO_2 photoreduction route are shown in Fig. 3. First, the hydroxyl group of H_2O will react with the hydrogen in the C-OH group of TEOA to form a C-O- site [38] through an exothermic reaction, which is consistent with the above structural calculation results. CO_2 will be adsorbed on the C-O- sites formed in the previous step. Typically, *COOH and *CO intermediates are formed by the reaction of multiple electrons and protons, causing two reaction paths in *CO: (1) desorption of adsorbed *CO to form the final product CO; (2) *CO is further hydrogenated to form the *CHO intermediate and converted to CH_4 through a multistep protonation reaction. Due to the presence of the *CHO intermediate in in-situ FTIR and the lower Gibbs free energy for *CO to hydrogenize, it is more conducive for the formation of CHO than CO desorption. There was no $*CH_3OH$ signal in the in situ FTIR, indicating that the $*CH_2OH$ intermediate was not further hydrogenated to form $*CH_3OH$ but instead was hydrogenated and released water molecules to form the $*CH_2$ intermediate, which was then hydrogenated to release CH_4. Although the formation of CH_4 is more thermodynamically favorable according to the lower energy for *CO hydrogenation, the yield of CO is higher in actual photocatalytic experiments. Therefore, it can be speculated that there is another undisclosed reaction pathway of TEOA to generate CO. Under light irradiation, especially ultraviolet light, the covalent bond may undergo homolysis in many organic chemical reactions. [39–41] Since TEOA does not undergo self-decomposition, homolysis of chemical intermediates is more likely to occur due to weaker bond strength. It can be speculated that there may be bond homolysis induced by UV light. RO-COOH intermediates are formed after the chemisorption of CO_2 and following the hydrogenation process, which is confirmed by the in-situ FTIR results. The covalent bond in RO-COOH can be homogenized under the induction of UV light, resulting in·COOH. The·COOH radical can produce CO through a hydrogen atom transfer (HAT) process (Fig. 4a). The transfer pathway of the HAT process can be clarified by replacing H_2O with D_2O.

3.4. Hydrogen atom transfer (HAT)

The hydrogen atoms in D_2O have a larger atom weight, making a more difficult HAT process. As shown in Fig. S11, the production performance of CO decreased, indicating a slower rate for the HAT process of·COOD in D_2O.·COOD radicals generated by UV-excited homolysis are intermediates in the production pathway of CO. A schematic diagram of the reaction is shown in Fig. 4a. Homolysis occurs under illumination to form RO- and carboxyl radicals after the formation of RO-COOH. Then, the carboxyl radicals undergo a HAT process with hydrogen atoms in water to finally generate CO. To verify the feasibility of the above path, the calculation results of Gibbs free energy are shown in Fig. 4b. *COOH is more prone to homolytic cleavage to generate carboxyl radicals, followed by a smooth HAT reaction finally generating H_2O and CO.

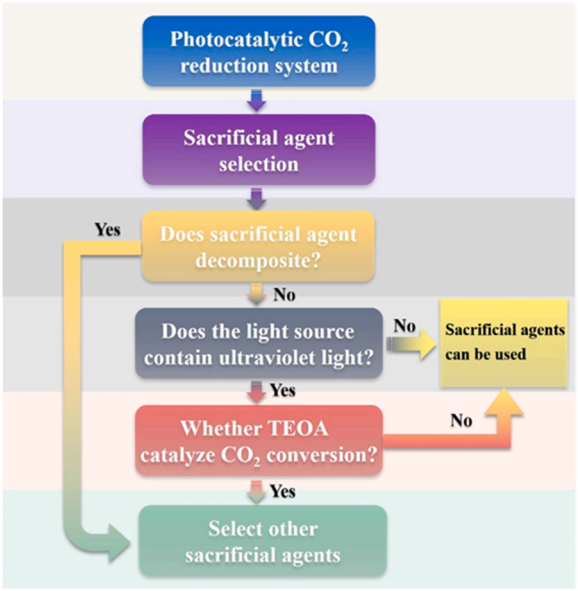

Fig. 5. Flow diagram of suggested protocols to select sacrificial agents.

According to the Gibbs free energy in the two whole routes, CO production via the photoinduced radical process is more likely to occur than the photocatalytic reduction pathway due to the lower energy barrier of 2.02 eV in Fig. 4 than 3.75 eV in Fig. 3, consistent well with the results of CO_2 photoreduction. Moreover, the wavelength of ultraviolet light used can meet the energy requirements of the two proposed paths for CO production. Therefore, it can be concluded that TEOA can catalyze CO_2 conversion to form CH_4 and CO via a conventional photocatalytic CO_2 hydrogenation route and photoinduced homocleavage of RO-COOH followed by a hydrogen atom transfer (HAT) process, respectively.

At last, considering the photocatalytic influence of TEOA on CO_2 conversion under UV light illumination, some preliminary guidances are provided to avoid the adverse effects of sacrificial agents on the evaluation of catalysts and exploration of the reaction mechanism (Fig. 5). When choosing the sacrificial agent for photocatalytic CO_2 reduction, it is necessary to eliminate the self-decomposition of the selected sacrificial agent. Next, it is necessary to determine whether the photocatalytic light source used contains ultraviolet light. The use of TEOA as a sacrificial agent is reasonable and acceptable in cases where the light source does not contain UV light. However, it is recommended to carry out further comparative experiments to determine whether TEOA catalyzes CO_2 conversion when UV light is present. The reliability of the experimental results can only be guaranteed under the experimental conditions that exclude the catalytic activity of TEOA; otherwise, it is recommended to use sacrificial agents other than TEOA.

4. Conclusions

In summary, we prove that TEOA could catalyze the reduction of CO_2 to CH_4 and CO under UV light illumination. Combined with in-situ Fourier transform infrared and DFT calculations, the terminal hydroxyl group in TEOA is corroborated to be the active site for CO_2 conversion. The two products of CH_4 and CO are derived from conventional photocatalytic CO_2 hydrogenation and photoinduced homocleavage of RO-COOH followed by a hydrogen atom transfer (HAT) process, respectively. It is anticipated that this work could attract researchers' attention to sacrificial agents and provide useful guidance for selecting suitable sacrificial agents in CO_2 photoreduction.

CRediT authorship contribution statement

Zhi-Guo Liu: Visualization, Data curation, Formal analysis, DFT calculations and wrote the manuscript. **Zi-Yu Chen**: DFT calculations. **Ming-Yang Li:** Software. **Jia-Ying Li:** Software. **Ling-Zhi Wang**: Writing – review & editing. **Shi-Qun Wu**: Writing – review & editing. **Jin-Long Zhang**: Visualization, Formal analysis, Review, Funding acquisition. All authors commented on the manuscript.

Declaration of Competing Interest

We have no known competing financial interests or personal relationships that could have appeared to influence the work reported in this paper.

Data Availability

Data will be made available on request.

Acknowledgements

This work was supported by the National Key R&D Program of China (2022YFE0107900, 2022YFB3803600), the National Natural Science Foundation of China (21972040, 21673073, 22202070), the Innovation Program of Shanghai Municipal Education Commission (2021–01-07–00-02-E00106), the Science and Technology Commission of Shanghai Municipality (20DZ2250400, 22230780200), the Project supported by Shanghai Municipal Science and Technology Major Project (No. 2018SHZDZX03), the Program of Introducing Talents of Discipline to Universities (No. B20031, B16017), the Postdoctoral Innovative Talent Support Program (BX20220107), and the Shanghai Rising-Star Program (22YF1410200).

Appendix A. Supporting information

Supplementary data associated with this article can be found in the online version at doi:10.1016/j.apcatb.2022.122338.

References

[1] Z. Liang, C. Qu, W. Guo, R. Zou, Q. Xu, Pristine metal-organic frameworks and their composites for energy storage and conversion, Adv. Mater. 30 (2018) 1702891.
[2] Y. Xia, J. Yu, Reaction: rational design of highly active photocatalysts for CO_2 conversion, Chem 6 (2020) 1039–1040.
[3] J. Fu, K. Jiang, X. Qiu, J. Yu, M. Liu, Product selectivity of photocatalytic CO_2 reduction reactions, Mater. Today 32 (2020) 222–243.
[4] S. Chu, Y. Cui, N. Liu, The path towards sustainable energy, Nat. Mater. 16 (2017) 16–22.
[5] C. Vogt, M. Monai, G.J. Kramer, B.M. Weckhuysen, The renaissance of the Sabatier reaction and its applications on Earth and in space, Nat. Catal. 2 (2019) 188–197.
[6] J. He, ky, C. Janá, Recent advances in solar-driven carbon dioxide conversion: expectations versus reality, ACS Energy Lett. 5 (2020) 1996–2014.
[7] A. Wagner, C.D. Sahm, E. Reisner, Towards molecular understanding of local chemical environment effects in electro-and photocatalytic CO_2 reduction, Nat. Catal. 3 (2020) 775–786.
[8] M. Zhou, S. Wang, P. Yang, C. Huang, X. Wang, Boron carbon nitride semiconductors decorated with CdS nanoparticles for photocatalytic reduction of CO_2, ACS Catal. 8 (2018) 4928–4936.
[9] X. Jia, C. Hu, H. Sun, J. Cao, H. Lin, X. Li, S. Chen, A dual defect co-modified S-scheme heterojunction for boosting photocatalytic CO_2 reduction coupled with tetracycline oxidation, Appl. Catal. B (2022), 122232.
[10] H. Zhang, J. Wei, J. Dong, G. Liu, L. Shi, P. An, G. Zhao, J. Kong, X. Wang, X. Meng, Efficient visible-light-driven carbon dioxide reduction by a single-atom implanted metal-organic framework, Angew. Chem. Int. Ed. 128 (2016) 14522–14526.
[11] W. Wang, C. Deng, S. Xie, Y. Li, W. Zhang, H. Sheng, C. Chen, J. Zhao, Photocatalytic c-c coupling from carbon dioxide reduction on copper oxide with mixed-valence copper (I)/copper (II), J. Am. Chem. Soc. 143 (2021) 2984–2993.
[12] R. Das, S. Chakraborty, S.C. Peter, Systematic assessment of solvent selection in photocatalytic CO_2 reduction, ACS Energy Lett. 6 (2021) 3270–3274.
[13] L. Wang, B. Cheng, L. Zhang, J. Yu, In situ irradiated XPS investigation on S-scheme TiO_2@$ZnIn_2S_4$ Photocatalyst for efficient photocatalytic CO_2 reduction, Small 17 (2021) 2103447.
[14] S. Cao, M. Yang, A.O. Elnabawy, A. Trimpalis, S. Li, C. Wang, F. Göltl, Z. Chen, J. Liu, J. Shan, Single-atom gold oxo-clusters prepared in alkaline solutions

catalyse the heterogeneous methanol self-coupling reactions, Nat. Chem. 11 (2019) 1098–1105.
[15] S. Cao, B. Shen, T. Tong, J. Fu, J. Yu, 2D/2D heterojunction of ultrathin MXene/Bi_2WO_6 nanosheets for improved photocatalytic CO_2 reduction, Adv. Funct. Mater. 28 (2018) 1800136.
[16] X. Feng, Y. Pi, Y. Song, C. Brzezinski, Z. Xu, Z. Li, W. Lin, Metal-organic frameworks significantly enhance photocatalytic hydrogen evolution and CO_2 reduction with earth-abundant copper photosensitizers, J. Am. Chem. Soc. 142 (2020) 690–695.
[17] X. Jiao, Z. Chen, X. Li, Y. Sun, S. Gao, W. Yan, C. Wang, Q. Zhang, Y. Lin, Y. Luo, Defect-mediated electron-hole separation in one-unit-cell $ZnIn_2S_4$ layers for boosted solar-driven CO_2 reduction, J. Am. Chem. Soc. 139 (2017) 7586–7594.
[18] D. Zeng, H. Wang, X. Zhu, H. Cao, W. Wang, Y. Zhang, J. Wang, L. Zhang, W. Wang, Photocatalytic conversion of CO_2 to acetic acid by $CuPt/WO_3$: Chloride enhanced C-C coupling mechanism, Appl. Catal. B 323 (2023), 122177.
[19] C. Dong, C. Lian, S. Hu, Z. Deng, J. Gong, M. Li, H. Liu, M. Xing, J. Zhang, Size-dependent activity and selectivity of carbon dioxide photocatalytic reduction over platinum nanoparticles, Nat. Commun. 9 (2018) 1–11.
[20] B.J. Liu, T. Torimoto, H. Matsumoto, H. Yoneyama, Effect of solvents on photocatalytic reduction of carbon dioxide using TiO_2 nanocrystal photocatalyst embedded in SiO2 matrices, J. Photochem. Photobiol., A 108 (1997) 187–192.
[21] Y.X. Chen, Y.F. Xu, X.D. Wang, H.Y. Chen, D.B. Kuang, Solvent selection and Pt decoration towards enhanced photocatalytic CO_2 reduction over $CsPbBr_3$ perovskite single crystals, Sustain. Energ. Fuel. 4 (2020) 2249–2255.
[22] B. Zhao, J. Xu, Y. Liu, J. Fan, H. Yu, Amino group-rich porous g-C_3N_4 nanosheet photocatalyst: facile oxalic acid-induced synthesis and improved H_2-evolution activity, Ceram. Int. 47 (2021) 18295–18303.
[23] M. Zhang, W. Zhong, Y. Xu, F. Xue, J. Fan, H. Yu, Photoinduced synthesis of ultrasmall amorphous $NiWS_x$ nanodots for boosting photocatalytic H_2-evolution activity of TiO_2, J. Phys. Chem. Solids 149 (2021), 109796.
[24] H. Bosch, G. Versteeg, W.P.M. Van Swaaij, Gas-liquid mass transfer with parallel reversible reactions-I. Absorption of CO_2 into solutions of sterically hindered amines, Chem. Eng. Sci. 44 (1989) 2723–2734.
[25] E. Jorgensen, C. Faurholt, Reactions between carbon dioxide and amino alcohols. II. Triethanolamine, Acta Chem. Scand. 8 (1954) 1141–1144.
[26] N.Y. Huang, H. He, S. Liu, H.L. Zhu, Y.J. Li, J. Xu, J.R. Huang, X. Wang, P.Q. Liao, X.M. Chen, Electrostatic attraction-driven assembly of a metal-organic framework with a photosensitizer boosts photocatalytic CO_2 reduction to CO, J. Am. Chem. Soc. 143 (2021) 17424–17430.
[27] X.M. Cheng, X.Y. Dao, S.Q. Wang, J. Zhao, W.Y. Sun, Enhanced photocatalytic CO_2 reduction activity over NH_2-MIL-125 (Ti) by facet regulation, ACS Catal. 11 (2020) 650–658.
[28] V. Jeyalakshmi, R. Mahalakshmy, K.R. Krishnamurthy, B. Viswanathan, Photocatalytic reduction of carbon dioxide in alkaline medium on La modified sodium tantalate with different co-catalysts under UV-Visible radiation, Catal. Today 266 (2016) 160–167.
[29] R. Kuriki, K. Sekizawa, O. Ishitani, K. Maeda, Visible-light-driven CO_2 reduction with carbon nitride: enhancing the activity of ruthenium catalysts, Angew. Chem. Int. Ed. 54 (2015) 2406–2409.
[30] S. Sato, T. Morikawa, S. Saeki, T. Kajino, T. Motohiro, Visible-light-induced selective CO_2 reduction utilizing a ruthenium complex Electrocatalyst linked to ap-type nitrogen-doped Ta_2O_5 semiconductor, Angew. Chem. Int. Ed. 49 (2010) 5101–5105.
[31] S. Wang, J. Lin, X. Wang, Semiconductor–redox catalysis promoted by metal-organic frameworks for CO_2 reduction, Phys. Chem. Chem. Phys. 16 (2014) 14656–14660.
[32] T.H. Jeon, D. Monllor-Satoca, Gh Moon, W. Kim, Hi Kim, D.W. Bahnemann, H. Park, W. Choi, Ag (I) ions working as a hole-transfer mediator in photoelectrocatalytic water oxidation on WO_3 film, Nat. Commun. 11 (2020) 1–9.
[33] S. Melchers, J. Schneider, A.V. Emeline, D.W. Bahnemann, Effect of H_2O and O_2 on the adsorption and degradation of acetaldehyde on anatase surfaces-An in situ ATR-FTIR study, Catal 8 (2018) 417.
[34] S. Melchers, J. Schneider, D.W. Bahnemann, Isotopic studies on the degradation of acetaldehyde on anatase surfaces, Catal. Today 340 (2020) 318–322.
[35] S.I. Faßbender, J.J. Molloy, C. Mück-Lichtenfeld, R. Gilmour, Geometric E→Z isomerisation of alkenyl silanes by selective energy transfer catalysis: stereodivergent synthesis of triarylethylenes via a formal anti-Metallometallation, Angew. Chem. Int. Ed. 131 (2019) 18792–18799.
[36] J. Ran, M. Jaroniec, S.Z. Qiao, Cocatalysts in semiconductor-based photocatalytic CO_2 reduction: achievements, challenges, and opportunities, Adv. Mater. 30 (2018) 1704649.
[37] Q.W. Chen, M. Huang, S. Gong, C. Wang, Y. Yang, P. Jiang, P. Wang, L. Hu, E.D.T. A. Lewis, basic molecule as a highly active electrocatalyst for CO_2 reduction to CH_4, Angew. Chem. Int. Ed. 60 (2021) 23002–23009.
[38] D.R. Chambers, A. Juneau, C.T. Ludwig, M. Frenette, D.B. Martin, C-O bond cleavage of alcohols via visible light activation of cobalt alkoxycarbonyls, Organometallics 38 (2019) 4570–4577.
[39] S. Protti, D. Ravelli, M. Fagnoni, Designing radical chemistry by visible light-promoted homolysis, Trends Chem. 4 (2022) 305–317.
[40] D. Alpers, K.P. Cole, C.R. Stephenson, Visible light mediated aryl migration by homolytic C-N cleavage of aryl amines, Angew. Chem. Int. Ed. 57 (2018) 12167–12170.
[41] S. Gnaim, A. Bauer, H.-J. Zhang, L. Chen, C. Gannett, C.A. Malapit, D.E. Hill, D. Vogt, T. Tang, R.A. Daley, Cobalt-electrocatalytic HAT for functionalization of unsaturated C-C bonds, Nature 605 (2022) 687–695.